Journal of Magnetic Resonance 210 (2011) 228–232

Contents lists available at ScienceDirect

Journal of Magnetic Resonance

journal homepage: www.elsevier.com/locate/jmr

Destination state screening of active spaces in spin dynamics simulations

M. Krzystyniak, Luke J. Edwards, Ilya Kuprov *

Oxford e-Research Centre, University of Oxford, 7 Keble Road, Oxford OX1 3QG, UK

ARTICLE INFO

Article history:
Received 17 December 2010
Revised 4 March 2011
Available online 11 March 2011

Keywords:
State space restriction
Spin dynamics
Destination state screening
Spinach

ABSTRACT

We propose a novel avenue for state space reduction in time domain Liouville space spin dynamics simulations, using detectability as a selection criterion – only those states that evolve into or affect other detectable states are kept in the simulation. This basis reduction procedure (referred to as *destination state screening*) is formally exact and can be applied on top of the existing state space restriction techniques. As demonstrated below, in many cases this results in further reduction of matrix dimension, leading to considerable acceleration of many spin dynamics simulation types. Destination state screening is implemented in the latest version of the *Spinach* library (http://spindynamics.org).

1. Introduction

The direct product nature of spin operators means that the dimension of their matrix representation scales exponentially with spin system size. This severely limits current simulation capabilities. Recent research has however demonstrated [1–7] that many states in large spin systems are redundant and that polynomially scaling algorithms (recently implemented in the *Spinach* software library [8]) exist for many practically encountered simulation tasks.

The current version of *Spinach* uses four different methods for state space reduction:

1. *Interaction graph analysis* tailors the basis set using the analysis of interaction connectivity found in the system – very high order correlations as well as correlations between spins that are remote on the interaction graph are dropped from the basis [4].
2. *Symmetry pruning* (where applicable) utilises the observation that, in the Liouville space formulation of spin dynamics [9], most practical situations only require the fully symmetric irreducible representation of the symmetry group to be simulated [1,10].
3. *Zero track elimination* (ZTE) performs on-the-fly analysis of the simulation trajectory and drops unpopulated dimensions from the basis set [3].
4. *Liouvillian path tracing* (PT) uses graph-theoretical methods to identify disconnected subspaces in the state space, each of which may be propagated individually [1].

The efficiency and applicability of these methods depend on the problem at hand, but in common NMR and ESR cases they allow straightforward simulation of systems with 40+ spins (liquid state NMR) and 10+ spins (liquid state ESR), including accurate treatment of relaxation and chemical kinetics [8].

This paper suggests a further improvement to the methods listed above – we observe that only those spin system trajectories that pass through the detection state need in practice be simulated. All propagator group orbits other than the orbit generated by the detection state can thus be dropped. This procedure (called *destination state screening*) is shown in this paper to be formally exact and can be applied on top of existing state space restriction techniques. As demonstrated below, this results in a further reduction of matrix dimension and leads to a significant acceleration of many simulations.

2. Destination state screening

Given the high degree of reduction achieved by existing state space restriction techniques [1,3,4,8], further reduction must be based on different physical criteria. One such criterion is detectability – a given state that gets populated but never evolves into the detection state need not be simulated because it will never contribute to the result. This can be formally deduced from the fact that a simulation can be carried out *backwards*, by reverse propagating the detection state $\hat{S}$ under the Liouvillian $\hat{\hat{L}}$ and projecting it onto the initial state $\hat{\rho}_0$:

$$\begin{aligned} S(t) &= \langle \hat{S}|\mathrm{e}^{-\mathrm{i}\hat{\hat{L}}t}|\hat{\rho}_0\rangle = \mathrm{Tr}(\hat{S}^\dagger \mathrm{e}^{-\mathrm{i}\hat{\hat{L}}t}\hat{\rho}_0) = \mathrm{Tr}(\hat{\rho}_0\hat{S}^\dagger \mathrm{e}^{-\mathrm{i}\hat{\hat{L}}t}) \\ &= \mathrm{Tr}(\hat{\rho}_0[\mathrm{e}^{\mathrm{i}\hat{\hat{L}}t}\hat{S}]^\dagger) = \mathrm{Tr}([\mathrm{e}^{\mathrm{i}\hat{\hat{L}}t}\hat{S}]^\dagger\hat{\rho}_0) = \langle \mathrm{e}^{\mathrm{i}\hat{\hat{L}}t}\hat{S}|\hat{\rho}_0\rangle \end{aligned} \quad (1)$$

* Corresponding author. Fax: +44 1865 610612.
E-mail address: ilya.kuprov@oerc.ox.ac.uk (I. Kuprov).

1090-7807/$ - see front matter © 2011 Elsevier Inc. All rights reserved.
doi:10.1016/j.jmr.2011.03.010

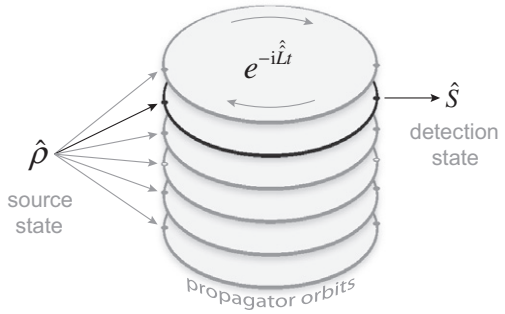

Fig. 1. Schematic illustration of destination state screening of time domain Liouville space spin dynamics simulations. The orbits induced in the system state space by the action of a given time propagator do not intersect and may be simulated separately. For a given initial state $\hat{\rho}_0$ and detection state $\hat{S}$, only the orbits containing contributions from *both* $\hat{\rho}_0$ and $\hat{S}$ need to be simulated.

This is a strictly equivalent simulation, meaning that the elements of $\hat{\rho}_0$ that are not reachable from $\hat{S}$ never contribute to $S(t)$. The corresponding state vectors can therefore be dropped from the basis set. Because $\hat{S}$ is often much simpler than $\hat{\rho}_0$ (particularly for complicated multi-stage pulse sequences), the dimension of the propagator group orbit of $\hat{S}$ is likely to be smaller than that of $\hat{\rho}_0$:

$$\mathrm{rank}\left\{\hat{S},\hat{P}\hat{S},\hat{P}^2\hat{S},\ldots,\hat{P}^n\hat{S}\right\}\leqslant\mathrm{rank}\left\{\hat{\rho}_0,\hat{P}\hat{\rho}_0,\hat{P}^2\hat{\rho}_0,\ldots,\hat{P}^n\hat{\rho}_0\right\}\tag{2}$$

where n is the number of points in the simulation trajectory. Application of existing trajectory level state space restriction tools [1,3,4,8] to $\hat{S}$ instead of $\hat{\rho}_0$ would thus lead to a greater degree of reduction. This is illustrated schematically in Fig. 1.

If the Liouvillian in Eq. (1) has anti-Hermitian terms (*e.g.* in the presence of relaxation or chemical processes), care must be taken to ensure that these anti-Hermitian superoperators do not change sign when the conjugate of the propagator is taken:

$$\begin{aligned}S(t)&=\langle\hat{S}|e^{-i\hat{L}t+\hat{R}t}|\hat{\rho}_0\rangle=\mathrm{Tr}(\hat{S}^\dagger e^{-i\hat{L}t+\hat{R}t}\hat{\rho}_0)\\&=\mathrm{Tr}(\hat{\rho}_0\hat{S}^\dagger e^{-i\hat{L}t+\hat{R}t})=\mathrm{Tr}(\hat{\rho}_0[e^{i\hat{L}t+\hat{R}t}\hat{S}]^\dagger)\\&=\mathrm{Tr}([e^{i\hat{L}t+\hat{R}t}\hat{S}]^\dagger\hat{\rho}_0)=\langle e^{i\hat{L}t+\hat{R}t}\hat{S}|\hat{\rho}_0\rangle\end{aligned}\tag{3}$$

The rest of this paper demonstrates that the reduction is indeed considerable in practice and tends to be particularly significant for the non-interacting subspace separation procedure [8] – not all independent subspaces detected by path tracing [1] contain the detection state. Many subspaces (often hundreds of them) cannot therefore evolve into being detected and need not be simulated in the first place. The sparsity of the detection state vector also tends to improve the efficiency of the ZTE procedure [3].

3. Example A: Isotropic pulse-acquire experiments

Our previous papers on the subject of state space restriction [1,3,4,8] have focused on NMR spectroscopy and Spin Chemistry; the majority of the examples presented below have thus been deliberately chosen from Electron Spin Resonance.

The flow of coherence through the state space of a methyl radical (a system that is small and simple enough for such diagrams) in a high-field isotropic pulse-acquire ESR experiment with a secular coupling Hamiltonian

$$\hat{H}=\sum_k\omega_k\hat{L}_Z^{(k)}+\sum_{nk}a_{nk}\hat{L}_Z^{(n)}\hat{L}_Z^{(k)}\tag{4}$$

is illustrated schematically in Fig. 2. Because both the initial and the detection states are located inside the A_1 (fully symmetric) irrep of the C_{3v} symmetry group and the time propagator $\exp(-i\hat{L}\Delta t)$ conserves the symmetry, any states outside A_1 can be dropped before the simulation starts. Once inside A_1, state space connectivity analysis [1] indicates that the initial state of the system $\hat{\rho}_0=\hat{L}_X\otimes\hat{E}\otimes\hat{E}\otimes\hat{E}$ (meaning $\hat{L}_X$ on the electron and unit operators on all three nuclei) populates only two four-dimensional and one one-dimensional propagator orbits out of 46: $\exp(-i\hat{L}t)(\hat{L}_+\otimes\hat{E}\otimes\hat{E}\otimes\hat{E})$, $\exp(-i\hat{L}t)(\hat{L}_-\otimes\hat{E}\otimes\hat{E}\otimes\hat{E})$ and the identity state (Table 1). The unpopulated orbits can be dropped, leaving us with 9-dimensional active space.

Destination state screening in this case amounts to noting that, of the two active orbits, only one orbit contains the quadrature detection state $\hat{S}=\hat{L}_+\otimes\hat{E}\otimes\hat{E}\otimes\hat{E}$. Therefore only one orbit should be kept. Of the original 256-dimensions this leaves a single 4-dimensional active space. These reductions are listed in the first two rows of Table 1. In addition one may introduce relaxation due

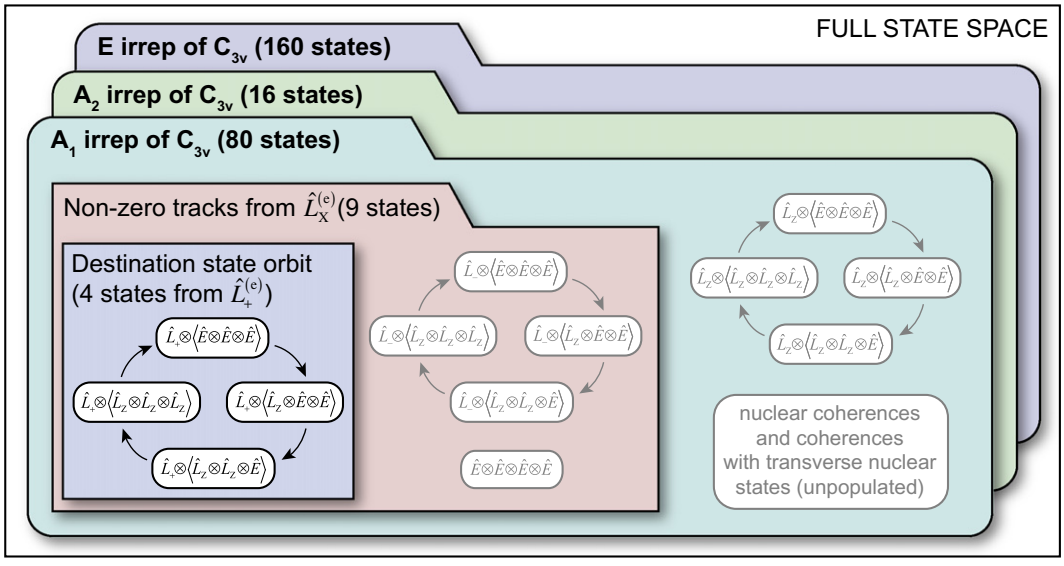

Fig. 2. Flowchart of the state space reduction procedure for the simple case of high-field liquid state ESR spectroscopy of a methyl radical. Of the three irreducible representations of the C_{3v} group, only A_1 is populated (256 → 80). Inside A_1, only electron coherences with longitudinal nuclear states are populated (80 → 9). Of the electron coherences that get populated by the initial state, only those belonging to the orbit that contains the quadrature detection state $\hat{L}_+^{(e)}$ need to be included in the basis (9 → 4).

Table 1
Matrix dimension statistics for time domain Liouville space simulations of the high-field pulse-acquire ESR experiment on several common organic radicals in the liquid state.

Radical and symmetry	Full state space dimension	Basis set[a]	Basis dimension	A_{1g} irrep dimension	Source state screening		Destination state screening	
					Dimension after ZTE	Dimension after ZTE and PT	Dimension after ZTE	Dimension after ZTE and PT
Methyl, S_3	256	*Complete*	256	80	9	$1 \times 1, 2 \times 4$	4	1×4
Methyl, S_1	256	*Complete*	256	256	19	$3 \times 1, 2 \times 8$	8	1×8
Phenyl, $S_2 \otimes S_2$	4096	*ESR*-1	128	72	39	$3 \times 1, 2 \times 18$	18	1×18
Pyrene, $S_4 \otimes S_4 \otimes S_2$	4×10^6	*ESR*-1	4096	300	153	$3 \times 1, 2 \times 75$	75	1×75
Chrysene, $\bigotimes_{n=1}^{6} S_2$	6×10^7	*ESR*-1	16,384	2916	1464	$6 \times 1, 2 \times 729$	729	1×729
Biaryl, $\bigotimes_{n=1}^{6} S_2$	3×10^8	*ESR*-1	36,864	5832	2922	$6 \times 1, 2 \times 1458$	1458	1×1458

[a] ESR-1 basis set: complete on the electrons, $\hat{T}_{l0}$ states only on nuclei, adapted to high-field ESR simulations [8].

to *g*-tensor and hyperfine tensor anisotropy using a secular Redfield superoperator [11,12]; in our case this was computed with the *Spinach* relaxation theory module [2,8]. The final active space dimension is then 10 – contributions from longitudinal spin orders also appear and the identity state gets connected to the active space.

In practice such analysis is done automatically. The clearest example is the Path Tracing procedure [8]: the state space is decomposed, using graph theory [1], into a set of subspaces that do not interact under the current Liouvillian. The detection state is then projected into the resulting subspaces and the projection norms are inspected. The subspaces that do not contain any part of the detection state would not contribute to the observed signal – they may be dropped. A similar argument can be made for the selection of trajectories based upon the application of Zero Track Elimination [3] to the detection state: as per Eq. (1), ZTE may be applied to the destination state instead of the initial state.

Examples of the reduction in matrix dimension achieved for larger systems are summarized in Table 1. Even for a biaryl radical (a 13-spin system, including two spin-1 ^{14}N nuclei), time-domain simulation in Liouville space is straightforward. The effect of destination state screening is in all cases to eliminate disconnected subspaces that do not produce or affect detectable magnetization. Note the full use of complicated direct product symmetries (including ^{14}N) – at the time of writing this feature remains unique to the *Spinach* library [8].

An NMR example is given in Fig. 3. The large *J* couplings in the 15-spin ^{19}F system of this perfluoroparacyclophane molecule [13] mean that the matrix dimension, even after state space restriction, symmetry factorization, and zero track elimination, is of the order of 3×10^4. Path tracing through the Liouvillian reveals that this space can be split into two independent subspaces of dimension $\sim 10^4$, and 15 subspaces of dimension 1. Use of the detection state (in this case a sum of $\hat{S}_+$ states of the ^{19}F; this corresponds to quadrature NMR detection) to screen the subspaces reveals that only one of the $\sim 10^4$ size subspaces contains the detection state, and thus only this subspace has to be propagated.

4. Example B: ESEEM and ENDOR experiments

The examples in Table 1 and Fig. 3 may be viewed as favourable – highly symmetric systems with isotropic couplings and single evolution periods are only encountered in liquid state experiments. This section describes more challenging simulations of single crystal ESEEM [14] spectra as well as solution Mims ENDOR [14–16] spectra. The results are in good agreement with experiment and are identically equal to those generated using exact simulations.

The results of applying state space restriction to the ESEEM simulation of several simple radicals are shown in Table 2. With anisotropic ESR systems, the previously published state space restriction methods [1,3,4,8] only produce modest improvements – they yield a block diagonalization, with the dimension of the largest block only a factor of four smaller than the full state space dimension. Application of destination state screening with respect to the quadrature detection state on the electron ($\hat{S}_+$) reveals that in fact only one block needs to be propagated. Because the central pulse in the ESEEM sequence is a simple inversion [14], one can also apply destination state screening to the first evolution period (using $\hat{S}_- = -\exp(i\pi\hat{S}_Y)\hat{S}_+$ as the destination state) leading to the same degree of reduction as for the final evolution period.

The improvement achieved for liquid-state ENDOR experiments is quite dramatic (Table 3): only one tiny subspace survives in the final evolution period, and the largest matrix dimension encountered anywhere in the simulation is typically a factor of twenty smaller than the full state space dimension. The result is, of course, identical to that produced by the exact simulation.

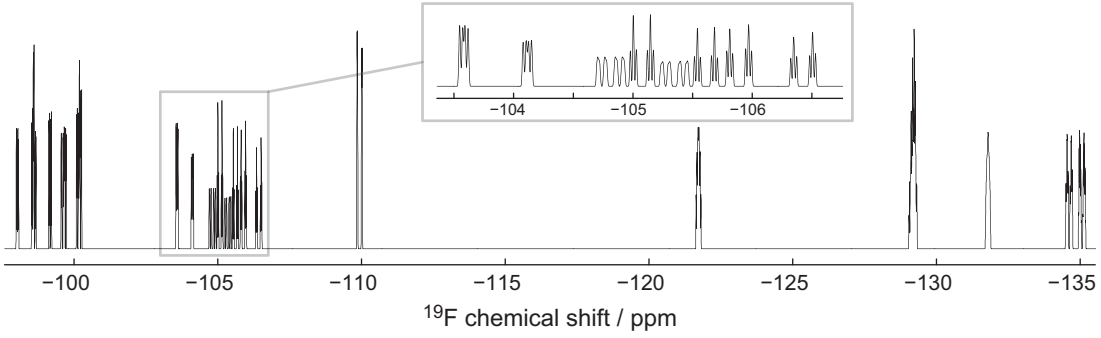

Fig. 3. Simulation of the ^{19}F NMR spectrum of a 15-spin perfluoroparacyclophane molecule. The IK-2 basis set was used (for every spin the spin orders involving directly coupled spins are kept [8]). Chemical shifts and coupling constants are taken from [13]. The Liouville space dimension of $\sim 10^9$ is reduced by existing state space restriction methods to $\sim 3 \times 10^4$. Destination state screening reveals that only a third of this space has to be propagated in order to simulate the spectrum.

Table 2
Matrix dimension statistics for time domain Liouville space simulations of the high-field ESEEM experiment on common organic radicals in the solid state (random orientation[a]).

Radical	State space dimension	Source state screening		Destination state screening	
		Dimension after ZTE	Dimension after ZTE and PT	Dimension after ZTE	Dimension after ZTE and PT
^{15}N-TEMPOL	16	14	2×4, 1×6	4	1×4
Methyl	256	146	3×6, 2×64	64	1×64
Phenyl	4096	2078	5×6, 2×1024	1024	1×1024

[a] Hyperfine and *g*-tensors obtained from a DFT B3LYP/EPR-II calculation using Gaussian03.

5. Example C: 2D NMR experiments

Simulations of 2D NMR sequences (COSY, NOESY, HSQC, HMQC, HETCOR, *etc.* are currently included with *Spinach*), tend to benefit considerably from destination state screening (Table 4). This is because the state vector becomes densely populated by the time the sequence enters the F2 detection period, but the quadrature detection state is always just a sum of $\hat{S}_+$ states on all nuclei of the specified type. Of the large number of independent subspaces that get populated at the final stage of these sequences, very few survive the screening.

6. Summary and outlook

The destination state screening procedure introduced above uses detectability as a basis truncation criterion – subspaces of the state space that neither lead to, nor contribute to the simulation result are dropped. The result is further acceleration of many types of NMR and ESR simulations.

Extensions of this technique are possible – one can imagine screening against different non-conventional observables used in exotic detection schemes (*e.g.* longitudinal detection in ESR [17] and optical detection of singlet yield in Spin Chemistry [18]), or screening against multiple quantum coherence states within complex pulse sequences. With case-specific knowledge of individual pulse sequences, it should be possible to apply the screening at simulation stages that do not necessarily involve detection – if one has the knowledge of how the different subspaces feed into each other throughout the pulse sequence, it should be possible to set up screens for each evolution period, threading the (eventually) observable magnetization through several "keyholes" along the way.

Table 3
Matrix dimension statistics for time domain Liouville space simulations of the high-field Mims ENDOR experiment on common organic radicals in the liquid state.

Radical and symmetry	State space dimension	A_{1g} irrep dimension	First evolution period, after ZTE and PT	Second evolution period, after ZTE and PT	Third evolution period, source state screening		Third evolution period, destination state screening	
					Dimension after ZTE	Dimension after ZTE and PT	Dimension after ZTE	Dimension after ZTE and PT
^{15}N-TEMPOL	16	16	1×1, 2×2	5×1, 2×2	16	5×1, 4×2	2	1×2
Methyl, S_3	256	80	1×1, 2×4	10×1, 10×2, 4×3, 2×4	80	14×1, 12×2, 4×3, 2×4	4	1×4
Phenyl, $S_2 \otimes S_2$	4096	1600	3×1, 2×18	40×1, 120×1, 24×3, 40×4, 28×6 8×8, 4×9, 8×12, 2×18	1600	70×1, 240×2, 24×3, 40×4, 28×6, 8×8, 4×9, 8×12, 2×18	18	1×18

Table 4
Matrix dimension statistics for time domain Liouville space simulations of 2D NMR experiments on common spin systems in the liquid state.

Spin system and pulse sequence	Liouville space dimension	Basis[a] dimension	F1 evolution period, after ZTE and PT	Mixing time, after ZTE and PT	F2 evolution period, source state screening		F2 evolution period, destination state screening	
					Dimension after ZTE	Dimension after ZTE and PT	Dimension after ZTE	Dimension after ZTE and PT
Strychnine, ^{1}H NOESY	1.8×10^{13} (22 spins)	6511	2×26, 2×56, 2×1152	1×178	6511	219×1, 6×8, 2×10, 2×11, 2×12, 2×26, 2×28, 2×56, 2×66, 2×278, 2×707, 2×1173, 1×1510	1241	1×26, 1×56, 1×1152
Sucrose, ^{1}H DQF–COSY	1.8×10^{13} (22 spins)	1516	5×1, 1×4, 1×78, 1×171	–	1516	394×1, 3×4, 4×8, 2×15, 2×38, 2×78, 2×87, 2×94, 2×171, 1×206	258	5×1, 1×4, 1×78, 1×171
Rotanone,^{1}H COSY-45	1.8×10^{13} (22 spins)	985	18×1, 2×15, 4×97	–	985	43×1, 2×6, 6×15, 1×18, 4×50, 4×97, 2×117	218	9×1, 1×15, 2×97
Strychnine, ^{1}H–^{13}C HSQC[b]	7.7×10^{25} (43 spins)	16,906	21×1, 4×2, 2×8, 2×12, 2×16, 2×34, 2×144, 2×200, 2×266	–	634	58×1, 9×4, 4×6, 9×7, 2×8, 2×11, 4×15, 2×18, 2×26, 2×28, 1×31, 2×56, 1×68	126	2×1, 3×4, 2×15. 1×26, 1×56

[a] IK-2 basis set: includes, for each spin, all spin orders with its nearest neighbours on the interaction graph [8].
[b] Analytical decoupling – all scalar ^{1}H–^{13}C couplings are set to zero during the F2 detection period. ^{13}C nuclei are assumed to be dilute.

Acknowledgments

The authors would like to thank Gareth Charnock, Hannah Hogben and Peter Hore for stimulating discussions. The Project is funded by the EPSRC (EP/F065205/1, EP/H003789/1) and supported by the Oxford e-Research Centre.

References

[1] H.J. Hogben, P.J. Hore, I. Kuprov, Strategies for state space restriction in densely coupled spin systems with applications to spin chemistry, J. Chem. Phys. 132 (2010) 174101.
[2] I. Kuprov, Diagonalization-free implementation of spin relaxation theory for large spin systems, J. Magn. Reson. 209 (2011) 31–38.
[3] I. Kuprov, Polynomially scaling spin dynamics II: further state-space compression using Krylov subspace techniques and zero track elimination, J. Magn. Reson. 195 (2008) 45–51.
[4] I. Kuprov, N. Wagner-Rundell, P.J. Hore, Polynomially scaling spin dynamics simulation algorithm based on adaptive state-space restriction, J. Magn. Reson. 189 (2007) 241–250.
[5] M.C. Butler, J.N. Dumez, L. Emsley, Dynamics of large nuclear-spin systems from low-order correlations in Liouville space, Chem. Phys. Lett. 477 (2009) 377–381.
[6] J.N. Dumez, M.C. Butler, E. Salager, B. Elena-Herrmann, L. Emsley, Ab initio simulation of proton spin diffusion, Phys. Chem. Chem. Phys. 12 (2010) 9172–9175.
[7] A.M. Castillo, L. Patiny, J. Wist, Fast and accurate algorithm for the simulation of NMR spectra of large spin systems, J. Magn. Reson. 208 (2011) 123–130.
[8] H.J. Hogben, M. Krzystyniak, G.T.P. Charnock, P.J. Hore, I. Kuprov, Spinach – a software library for simulation of spin dynamics in large spin systems, J. Magn. Reson. 208 (2011) 179–194.
[9] A.D. Bain, J.S. Martin, FT NMR of nonequilibrium states of complex spin systems. I. A Liouville space description, J. Magn. Reson. 29 (1978) 125–135.
[10] F.P. Temme, Symmetry-adapted bases over Liouville space. IV. Projection superoperators and invariance hierarchies for and [X] groups: a characterization of [A]4 and [AX]4 spin systems, Chem. Phys. 132 (1989) 9–30.
[11] M. Goldman, Formal theory of spin-lattice relaxation, J. Magn. Reson. 149 (2001) 160–187.
[12] A.G. Redfield, On the theory of relaxation processes, IBM J. Res. Dev. 1 (1957) 19–31.
[13] I. Ghiviriga, L. Zhang, H. Martinez, R.H. Contreras, C.F. Tormena, L. Nodin, W.R. Dolbier, 19F chemical shifts, coupling constants and conformational preferences in monosubstituted perfluoroparacyclophanes, Magn. Reson. Chem. 49 (2011) 93–105.
[14] A. Schweiger, G. Jeschke, Principles of pulse electron paramagnetic resonance, Oxford University Press, Oxford, 2001.
[15] P. Höfer, A. Grupp, M. Mehring, High-resolution time-domain electron-nuclear-sublevel spectroscopy by pulsed coherence transfer, Phys. Rev. A 33 (1986) 3519–3522.
[16] H. Cho, Stimulated echo time domain electron nuclear double-resonance, J. Chem. Phys. 94 (1991) 2482–2495.
[17] J. Granwehr, J. Forrer, A. Schweiger, Longitudinally detected EPR: improved instrumentation and new pulse schemes, J. Magn. Reson. 151 (2001) 78–84.
[18] A.L. Buchachenko, Recent advances in spin chemistry, Pure Appl. Chem. 72 (2000) 2243–2258.